Journal of Dynamics, Monitoring and Diagnostics, 2025, 4, 194-202
https://doi.org/10.37965/jdmd.2025.885

ISTP
RESEARCH ARTICLE

Investigations on Multiclass Classification Model-Based Optimized Weights Spectrum for Rotating Machinery Condition Monitoring

Bingchang Hou,[1] Yu Wang,[2] and Dong Wang[2]
[1]State Key Laboratory of Mechanical Transmission for Advanced Equipment, Chongqing University, Chongqing, China
[2]Department of Industrial Engineering and Management, School of Mechanical Engineering, Shanghai Jiao Tong University, Shanghai, P.R. China

(Received 30 July 2025; Revised 21 August 2025; Accepted 04 September 2025; Published online 05 September 2025)

Abstract: Machinery condition monitoring is beneficial to equipment maintenance and has been receiving much attention from academia and industry. Machine learning, especially deep learning, has become popular for machinery condition monitoring because that can fully use available data and computational power. Since significant accidents might be caused if wrong fault alarms are given for machine condition monitoring, interpretable machine learning models, integrate signal processing knowledge to enhance trustworthiness of models, are gradually becoming a research hotspot. A previous spectrum-based and interpretable optimized weights method has been proposed to indicate faulty and fundamental frequencies when the analyzed data only contains a healthy type and a fault type. Considering that multiclass fault types are naturally met in practice, this work aims to explore the interpretable optimized weights method for multiclass fault type scenarios. Therefore, a new multiclass optimized weights spectrum (OWS) is proposed and further studied theoretically and numerically. It is found that the multiclass OWS is capable of capturing the characteristic components associated with different conditions and clearly indicating specific fault characteristic frequencies (FCFs) corresponding to each fault condition. This work can provide new insights into spectrum-based fault classification models, and the new multiclass OWS also shows great potential for practical applications.

Keywords: machinery condition monitoring; optimized weights spectrum; spectrum analysis; softmax classifier; interpretable machine learning model

I. INTRODUCTION

Machinery condition monitoring [1] could provide machinery health information, such as incipient fault time, fault types, and remaining useful life, which are beneficial to avoiding sudden machinery breakdown and human injury, increasing industrial economic profits. Therefore, machinery condition monitoring has received much research attention from both academia and industry. The essence of machinery condition monitoring is to extract key fault information by analyzing monitored data [2]. Vibration signals contain much health state information, and they might be the most common data type to be analyzed [3]. A variety of rotating components, such as bearings and gears, are employed to support mechanical rotating bodies or to transmit torque. Thus, these rotating parts are prone to faults, and more research attention has been put on them. In general, monitoring strategies fall into two major categories: signal processing approaches and data-driven learning approaches.

Signal processing methods mainly use techniques including the Fourier transform, Hilbert transform [4], time-frequency analysis, bandpass filtering, and signal decompositions [5]. Due to the periodic impacts between defective and intact rotating elements, the vibration signals under fault conditions often exhibit repetitive impulsive transients, which are regarded as typical fault-related features. The impulsive repetitive transients introduced by rotating mechanical faults have several significant features that could be utilized to design signal processing methods: (***i***) If a rotating part works under a constant speed, the time distance of each transient in repetitive fault transients is approximately periodic, and the reciprocal of the time distance represents the appearance frequency of each transient. Since impulsive fault transients of different rotating mechanical faults usually have unique appearance frequencies, this appearance frequency is called the fault characteristic frequency (FCF) and could be calculated from mechanical structural parameters. In addition, the signal processing method known as order tracking [6] has been developed for analyzing fault vibration signals obtained under variable-speed operating conditions, where the corresponding frequency manifestation is referred to as the fault characteristic order (FCO). Through the application of a Hilbert transform-based envelope demodulation technique [4], the FCF or FCO, together with their harmonics, can be extracted from the envelope spectrum or the squared envelope spectrum (SES). Spectral correlation [7] and its fast implementation [8] are also studied and applied to the identification of FCFs. (***ii***) When fault vibration signals are transformed to the frequency domain using the Fourier transform, the impulsive repetitive transients are usually located in some specific frequency bands (being called informative frequency bands), so methods having a

Corresponding author: Yu Wang (e-mail: wangyusjtu2022@sjtu.edu.cn).

bandpass filtering property are often designed to filter raw signals containing other interferential components. Two pioneering works for this purpose are fast Kurtogram [9] and minimum entropy deconvolution [10], respectively. Later, improved variants of the two pioneering works gradually became a hot research topic [11, 12]. General signal decomposition methods having a bandpass filtering property, such as the empirical mode decomposition (EMD) and variational mode decomposition (VMD), are also introduced for machinery condition monitoring. However, researchers recently noticed the performance restriction of these general decomposition methods [13, 14], and more tailored signal decomposition methods are being developed for machinery condition monitoring. For instance, Miao *et al*. proposed a feature mode decomposition [15] by improving a maximum correlated kurtosis deconvolution (MCKD), and Hou *et al*. designed an impulsive mode decomposition (IMD) [16] by using new cycle-embedded sparsity measures (CESM) [17] as the objective function of a new iterative frequency band searching model. Signal-processing-based methods are usually designed according to the characteristics of the analyzed machinery fault signals, so their interpretability is strong. However, the restriction of signal processing methods lies in that they are designed to analyze specific kinds of data, but they lack the ability to handle variable tasks. Signal components/features extracted by signal processing methods should be integrated with machine learning techniques to train models for incipient fault time detection, fault classification, and remaining useful life prediction.

Machine learning methods [18] applied to machinery condition monitoring include the expert system, support vector machine (SVM), decision tree, neural network-based deep learning, etc., among which the deep learning methods [19] have gradually reformed intelligent methods for machinery condition monitoring since the 2010s. For example, Guo *et al*. [20] proposed a recurrent neural network-based approach to construct a health index was designed to predict the residual service life of bearings. Shao *et al*. [21] introduced a transfer learning-based deep model for diagnosing faults in rotating machinery such as motors, gearboxes, and bearings. The machine learning methods, especially deep learning, have great ability in extracting advanced abstract fault features and training models, but their interpretability is usually insufficient, and the extracted fault features cannot directly manifest physical connections with intuitive fault features such as FCF exhibited in the SES and selected frequency bands of the Fourier domain. However, practical machinery condition monitoring is a highly sensitive task, i.e., a delayed fault alarm may cause significant accidents. Thus, interpretable intelligent machinery condition monitoring methods, which can increase methods' credibility and reliability and further help algorithm improvement and diagnostic result attribution, are gradually receiving more and more research attention in recent several years.

Signal processing knowledge is an important inspiration for designing interpretable machine learning-based machinery condition monitoring methods. For instance, based on wavelet transform, Li *et al*. [22] formulated an interpretable WaveletKernelNet method by using a continuous wavelet convolutional (CWConv) layer as a replacement for the first layer of a standard convolutional neural network. Wang *et al*. [23] designed an algorithm unrolling an adversarial network to detect anomaly mechanical faults, and the network structure is composed of an encoder and a decoder, which is established by unrolling a sparse coding model. Chen *et al*. [24] proposed a time-frequency network by embedding the physically interpretable time-frequency transform into a traditional trainable convolutional layer. Though these methods incorporated signal processing knowledge into neural networks, intuitive connections between model weight parameters or extracted advanced features with physically interpretable fault features (e.g., informative frequency bands, FCFs, or FCOs) are still lacking. As discussed above, the FCFs and informative frequency bands have strong connections with specific fault types, so if model parameters or extracted features have strong connections with them, the diagnostic or condition monitoring results can be effectively supported. Fortunately, a recent series of studies proposed a new spectrum machine learning method by solving a two-class classification model, named sum of weighted normalized Fourier spectrum/SES (SWNSES or SWNFS) [25–27]. Mathematical analysis [27] proved that the model weight parameters can indicate fundamental frequency components, informative frequency bands, or FCFs and their harmonics, having a strong interpretability. Further, the accordingly interpretable model weight parameters are called optimized weight spectrum (OWS), and new fault feature extraction methods, such as OWS-based index [28], optimized weight time–frequency matrix index [29], difference mode decomposition [30], Differgram [31], spectral feature-informed difference multi-modes decomposition [32], robust optimized weight spectrum [33], etc., are designed for machinery condition monitoring.

Overall, it is practically significant to explore more interpretable machine learning-based machinery condition monitoring methods, which is also the focus of this article. Considering that the interpretable OWS is derived from the two-class classification model (e.g., linear SVM, logistic regression), and multiclass classification model (e.g., softmax classifier) is a natural extension of the two-class classification model and has been widely applied to fault classification methods, it is meaningful to investigate the interpretability of similar weight parameters. This research makes the following contributions:

(1) The binary-class classification model-based OWS is extended to a multiclass classification model-based OWS. Thus, new multiclass OWS is acquired.

(2) Softmax classifier is used to solve the multiclass OWS, and the interpretability of the multiclass OWS is studied and theoretically proved. It can be shown that, in the multiclass OWS, positive spectral lines correspond to the characteristic components associated with a specific class, while negative spectral lines reflect either interferential components or fault components from other classes.

(3) Numerical and experimental cases validated the interpretable properties of the multiclass OWS. It further demonstrates that the multiclass OWS can effectively capture the discriminative spectral differences among various health conditions, thereby facilitating practical and reliable fault diagnosis and condition monitoring.

The paper is organized as follows: Section II provides a review of earlier OWS studies based on binary classification models. Section III first details the idea and algorithm of OWS based on the multiclass classification model; then, the

physical interpretability of the multiclass OWS is theoretically investigated; finally, a numerical study is designed to validate the theoretical properties of the multiclass OWS. Section IV presents an experimental validation case using bearing datasets. Finally, Section V provides the conclusions of this paper.

II. PREVIOUS INTERPRETABLE OWS BASED ON BINARY CLASSIFICATION MODELS

In this part, we revisit the formulation of the OWS and its main characteristics. The OWS was initially developed to highlight fault-related spectral components, thereby offering insightful information for condition assessment and maintenance planning.

The procedure for implementing OWS can be described as follows. Suppose a signal as $\boldsymbol{x} \in \mathbb{R}^{N\times 1}$ where N is the length of the signal. Let $\boldsymbol{GS} = \mathrm{G}(\boldsymbol{x}) \in \mathbb{R}^{N\times 1}$ represent a generalized spectrum (GS) of a signal $\mathbf{x}$ with N points, obtained through a spectral transformation $\mathrm{G}(\cdot)$ such as Fourier spectrum, SES, or other signal representations. Then, a normalized generalized spectrum (NGS) can be calculated by $\boldsymbol{NGS} = \boldsymbol{GS}/\|\boldsymbol{GS}\|_1$. Suppose that M samples are gathered from both healthy and faulty states. These are organized into a dataset defined as $T = \{\boldsymbol{NGS}_{y_i,i}, y_i | \boldsymbol{NGS}_{y,i} \in \mathbb{R}^N, y_i \in \{0,1\}\}_{i=1}^{M}$, where $y_i = 0$ indicates a healthy condition and $y_i = 1$ denotes a faulty condition. In addition, significant spectral lines in $\boldsymbol{NGS}_{y_i,i}$ are defined as the characteristic components of class y_i, which serve as key features for condition identification. For binary classification, the normalized spectra are separated in the feature domain by constructing a hyperplane defined as

$$\boldsymbol{\omega}^T \boldsymbol{NGS} + b = 0, \tag{1}$$

with $\boldsymbol{\omega}$ representing the weight vector and b denoting the intercept of the hyperplane. To maximize the posterior separation between the two health conditions, an optimal decision function is learned based on maximum likelihood estimation (MLE) with L_2-regularization [26]:

$$\max L(\boldsymbol{\beta}) = \frac{1}{2M}\sum_{i=1}^{M}[y_i \boldsymbol{\beta}^T \boldsymbol{z}_i - \log(1+\exp(\boldsymbol{\beta}^T \boldsymbol{z}_i))] + \frac{1}{2M}\lambda \boldsymbol{\beta}^T \boldsymbol{\beta} \tag{2}$$

where $\boldsymbol{\beta} = [\boldsymbol{\omega}^T, b]$, $\boldsymbol{z}_i = [(\boldsymbol{NGS}_{y_i,i})^T, 1]^T$, and λ is a regularization coefficient. It is noteworthy that λ can be determined by Bayesian information criterion (BIC) [34]. Specifically, an expression of the BIC is as follows:

$$\mathrm{BIC} = -L(\boldsymbol{\beta}^*) + k\log(N), \tag{3}$$

where $\boldsymbol{\beta}^*$ is the optimal solution of (2); k is a degree of freedom, which is defined as the number of nonzero elements in $\boldsymbol{\beta}^*$. According to the BIC criterion, the regularization coefficient is determined by evaluating the BIC values over a candidate set of λ and selecting the one that achieves the minimum BIC.

Besides, SVM can also be applied to obtain the OWS [25]. Solving the above problem yields an optimal separating vector $\boldsymbol{\omega}^*$, which defines the OWS for binary classification.

From the viewpoint of maximizing separation between the two health states in feature space, the OWS can be understood as contrasting the normalized spectrum of a fault-related signal against that of a clean healthy signal, which has been proved in [27]. This interpretation reveals two essential characteristics of the OWS that enhance its ability in spectral fault analysis:

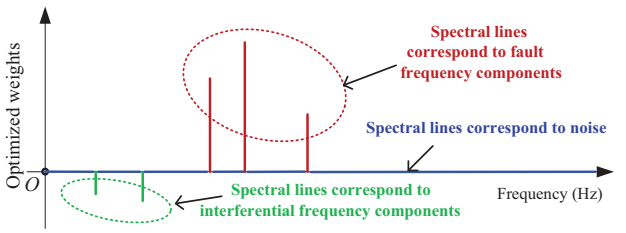

Fig. 1. Illustration of properties of an OWS.

(1) Locatable property: As shown in Fig. 1, the OWS accentuates spectral lines that are associated with various signal components. Specifically, positive-valued weight spectral lines indicate fault-related frequency components, negative-valued weight spectral lines reveal interfering components, and near-zero weight spectral lines correspond to noise. This property enables the precise localization of fault and non-fault information in the frequency domain.

(2) Amplitude property: The ratios between positive spectral amplitudes reflect the relative strengths of fault frequencies in the original signal. Similarly, the ratios among negative spectral amplitudes correspond to the proportional structure of interferential components.

III. NEW MULTICLASS INTERPRETABLE OWS BASED ON A MULTICLASS CLASSIFICATION MODEL

Although the two-class classification model-based OWS is effective in identifying characteristic components to distinguish healthy and faulty conditions, practical maintenance decision-making often considers multiple failure modes and constructs multiclass classification models. In practical industrial scenarios, a rotating machine may suffer from several different fault types simultaneously, and it is essential to distinguish not only faulty conditions from healthy ones but also different fault modes from each other. Simply combining multiple one-vs-rest binary classifiers is often insufficient, as such an approach may lead to inconsistent decision boundaries and, more importantly, may fail to capture the intrinsic differences among various fault types. In contrast, a direct multiclass formulation provides a unified framework that simultaneously handles all categories, avoids ambiguity, and enhances the physical interpretability of the resulting OWS. Therefore, it is very meaningful to explore the OWS based on multiclass classification models.

A. IDEA AND THE ALGORITHM IMPLEMENTATION

To extend the OWS to multiclass classification, a softmax classifier-based framework is adopted to separate the normalized spectra into K distinct machine health conditions. Let the dataset now consist of:

$$T = \{\boldsymbol{NGS}_{y_i,i}, y_i | \boldsymbol{NGS}_{y,i} \in \mathbb{R}^N, y_i \in \{0,1,\ldots,K-1\}\}_{i=1}^{M} \tag{4}$$

where y_i indicates the class label of signal i. A softmax classifier is then introduced to estimate the posterior probability of each health condition as

$$P(y_i = k|\boldsymbol{NGS}_i; \boldsymbol{W}, \mathrm{b}) = \frac{\exp(\boldsymbol{\omega}_k^T \boldsymbol{NGS}_i + b_k)}{\sum_{j=1}^{K} \exp(\boldsymbol{\omega}_j^T \boldsymbol{NGS}_i + b_j)} \tag{5}$$

where $\boldsymbol{W} = [\mathrm{w}_1, \ldots, \mathrm{w}_K] \in \mathbb{R}^{N\times K}$ and $\boldsymbol{b} \in \mathbb{R}^K$ are the model parameters. The parameters are learned by maximizing a likelihood function:

$$\max_{\mathbf{W},\mathbf{b}} L(\boldsymbol{W},\boldsymbol{b}) = \frac{1}{M}\sum_{i=1}^{M} \log P(y_i|\boldsymbol{NGS}_i) + \lambda \|\boldsymbol{W}\|_F^2 + \lambda \boldsymbol{b}^T \boldsymbol{b} \tag{6}$$

An optimal set of weight vectors $\{\boldsymbol{\omega}_k^*\}_{k=1}^K$ is obtained by solving this optimization problem, which defines multiclass OWS. Each weight vector corresponds to a direction in the spectral feature space that best separates a particular fault condition from the others.

To solve the optimization problem in multiclass OWS, a gradient-based iterative approach is adopted. The gradient of the regularized cross-entropy loss with respect to each class-specific weight vector $\boldsymbol{\omega}_k$ is given by

$$\frac{\partial L}{\partial \boldsymbol{\omega}_k} = \frac{1}{M}\sum_{i=1}^{M} \left[\delta(y_i = k) - P(y_i = k|\boldsymbol{NGS}_i)\right] \boldsymbol{NGS}_i + 2\lambda \boldsymbol{\omega}_k \tag{7}$$

where $\delta(\cdot)$ is an indicator function, and $P(y_i = k|\boldsymbol{NGS}_i)$ is the softmax probability. Similarly, the gradient with respect to the bias term b_k is

$$\frac{\partial L}{\partial \boldsymbol{b}_k} = \frac{1}{M}\sum_{i=1}^{M} \left[\delta(y_i = k) - P(y_i = k|\boldsymbol{NGS}_i)\right] + 2\lambda b_k \tag{8}$$

The parameters $(\boldsymbol{W},\boldsymbol{b})$ are updated using gradient descent until a convergence condition is achieved, and the new multiclass OWS can be obtained accordingly. Furthermore, the fault type can be identified according to the index k corresponding to the maximal posterior probability, which indicates the class to which the signal most likely belongs:

$$k^* = \mathrm{argmax}_k P(y_i = k|\boldsymbol{NGS}_i; \boldsymbol{W}, b) \tag{9}$$

where k^* denotes the predicted fault type.

B. RESEARCH ON THE PHYSICAL MEANINGS OF THE MULTIPLE-CLASS CLASSIFICATION MODEL-BASED OWS

In the original binary classification setting, the OWS obtained from a logistic classifier possesses clear interpretability [27]: the positive weights correspond to fault-related spectral components, while the negative weights reflect fundamental components that are contained in both healthy and faulty conditions. When extending to the multiclass setting, such as using a softmax classifier, each class-specific weight vector $\boldsymbol{\omega}_k$ plays an analogous role to the OWS in binary classification. Specifically, the Softmax classifier inherently decomposes into a series of one-vs-rest classification models, each separating class k from all other classes. The optimization model for $\boldsymbol{\omega}_k$ is as follows:

$$\begin{aligned} L^{(k)} &= \frac{1}{2M}\sum_{i=1}^{M}\left(y_i^{(k)} \log\left(\frac{e^{\boldsymbol{\beta}_k^T z_i}}{\sum_{j=1}^{K} e^{\boldsymbol{\beta}_j^T z_i}}\right) + (1-y_i^{(k)}) \log\left(1 - \frac{e^{\boldsymbol{\beta}_k^T z_i}}{\sum_{j=1}^{K} e^{\boldsymbol{\beta}_j^T z_i}}\right)\right) + \frac{1}{2M}\lambda \boldsymbol{\beta}_k^T \boldsymbol{\beta}_k \\ &= \frac{1}{2M}\sum_{i=1}^{M}\left(y_i^{(k)} \log\left(\frac{e^{\boldsymbol{\beta}_k^T z_i} / \sum_{j=1,j\neq k}^{K} e^{\boldsymbol{\beta}_j^T z_i}}{1 + e^{\boldsymbol{\beta}_k^T z_i} / \sum_{j=1,j\neq k}^{K} e^{\boldsymbol{\beta}_j^T z_i}}\right) + (1-y_i^{(k)}) \log\left(\frac{1}{1 + e^{\boldsymbol{\beta}_k^T z_i} / \sum_{j=1,j\neq k}^{K} e^{\boldsymbol{\beta}_j^T z_i}}\right)\right) + \frac{1}{2M}\lambda \boldsymbol{\beta}_k^T \boldsymbol{\beta}_k \\ &= \frac{1}{2M}\sum_{i=1}^{M}\left[y_i^{(k)} \boldsymbol{\beta}_k^T \boldsymbol{z}_i - \log\left(1 + e^{\boldsymbol{\beta}_k^T z_i}\right)\right] + \frac{1}{2M}\lambda \boldsymbol{\beta}_k^T \boldsymbol{\beta}_k. \end{aligned} \tag{10}$$

where $\boldsymbol{\beta}_k = \left[\boldsymbol{\omega}_k{}^T, b_k - \log\left(\sum_{j=1,j\neq k}^{K} e^{\boldsymbol{\beta}_j^T z_i}\right)\right]$ represents the weight vector of class k. It is noteworthy that the optimization model has an identical form to, which indicates the properties of the OWS can be extended to the multiple-class classification scenario. Following the research approach in [27], the $\boldsymbol{NGS}_k$ and $\boldsymbol{NGS}_j (j \neq k)$ are expected to become linearly separable in a high-dimensional space. Accordingly, the optimal linear hyperplane can be expressed as follows:

$$\boldsymbol{\omega}_k^{*T} \boldsymbol{NGS}_{y_i,i} + b_k^* - \log\left(\sum_{j=1,j\neq k}^{K} e^{\boldsymbol{\beta}_j^{*T} z_i}\right) = 0 \tag{11}$$

Denote $\boldsymbol{S}^{(k)}$ and $\boldsymbol{S}^{(\neg k)}$ are the ideal noiseless sample vectors (support vectors) to the optimal hyperplane, belonging to the class k and the other classes, respectively. To find the optimal linear hyperplane that can separate class k and other classes, one can develop the optimization model as follows:

$$\max_{\boldsymbol{\omega}_k} \boldsymbol{\omega}_k{}^T (\boldsymbol{S}^{(k)} - \boldsymbol{S}^{(\neg k)}) \quad s.t. \ \|\boldsymbol{\omega}_k\| = 1. \tag{12}$$

According to the conclusion in [27], the normalized multiclass OWS $\boldsymbol{\omega}_k / \|\boldsymbol{\omega}_k\|$, i.e., the optimal solution of, has a form of $(\boldsymbol{S}^{(k)} - \boldsymbol{S}^{(\neg k)}) / \|\boldsymbol{S}^{(k)} - \boldsymbol{S}^{(\neg k)}\|$. It is noteworthy that the multiclass OWS $\boldsymbol{\omega}_k$ can only measure differences between class k and other classes. To conduct a comprehensive analysis of the characteristic components across all

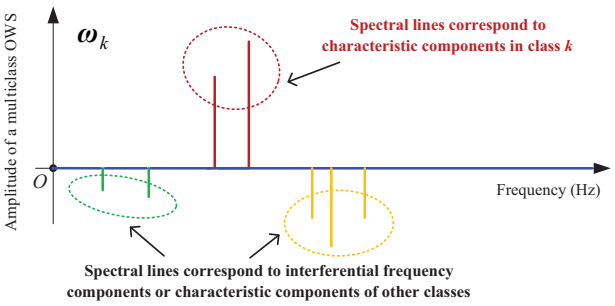

Fig. 2. Illustration of properties of a multiclass OWS.

K classes, a total of K OWS are required, i.e., each constructed by treating one class as the target and the remaining K−1 classes as the reference. Based on the above analysis results, it is concluded that a multiclass OWS has similar properties to the OWS for binary classification, which can be summarized as follows:

(1) Based on the interpretable K-class classification model shown in Section III.A, K interpretable OWS corresponding to one healthy condition and K-1 fault conditions could be acquired;

(2) For the interpretable OWS corresponding to the healthy condition, its positive weight spectral lines indicate interferential components (i.e., fundamental components) that are commonly present across all conditions, including both healthy and faulty states. In contrast, its negative spectral lines correspond to FCFs associated with the remaining K-1 faulty conditions.

(3) For an interpretable OWS corresponding to a specific faulty condition, it will exhibit positive weight spectral lines at the FCFs and be specific to that condition. Meanwhile, its negative weight spectral lines should arise from two sources: (i) FCFs associated with other faulty classes or (ii) common interferential components (i.e., fundamental components) that are not unique to the current fault.

As an illustration of Fig. 2, the physical meaning of the multiclass OWS is quite similar to the OWS for binary classification. The key difference between these two spectra lies in the meaning of the negative weights: they may originate not only from interferential components but also from the fault components of other classes.

C. NUMERICAL VALIDATIONS

To further validate the properties of the multiclass OWS, a numerical experiment is implemented with simulated bearing signals with pitting faults in different parts. According to the vibration model of rotating element bearings [35], the faulty bearing signals are regarded as periodic impulses convolved with the response of a single-degree-of-freedom (SDOF) system. Furthermore, the faulty bearing signals can be described x_k as follows:

$$x_k(t) = \sum_{i=1}^{\lfloor N/T_k \rfloor} A_k \delta(t - iT_k) * s_k(t) + B_r \cos(2\pi f_r t) + n(t), \tag{13}$$

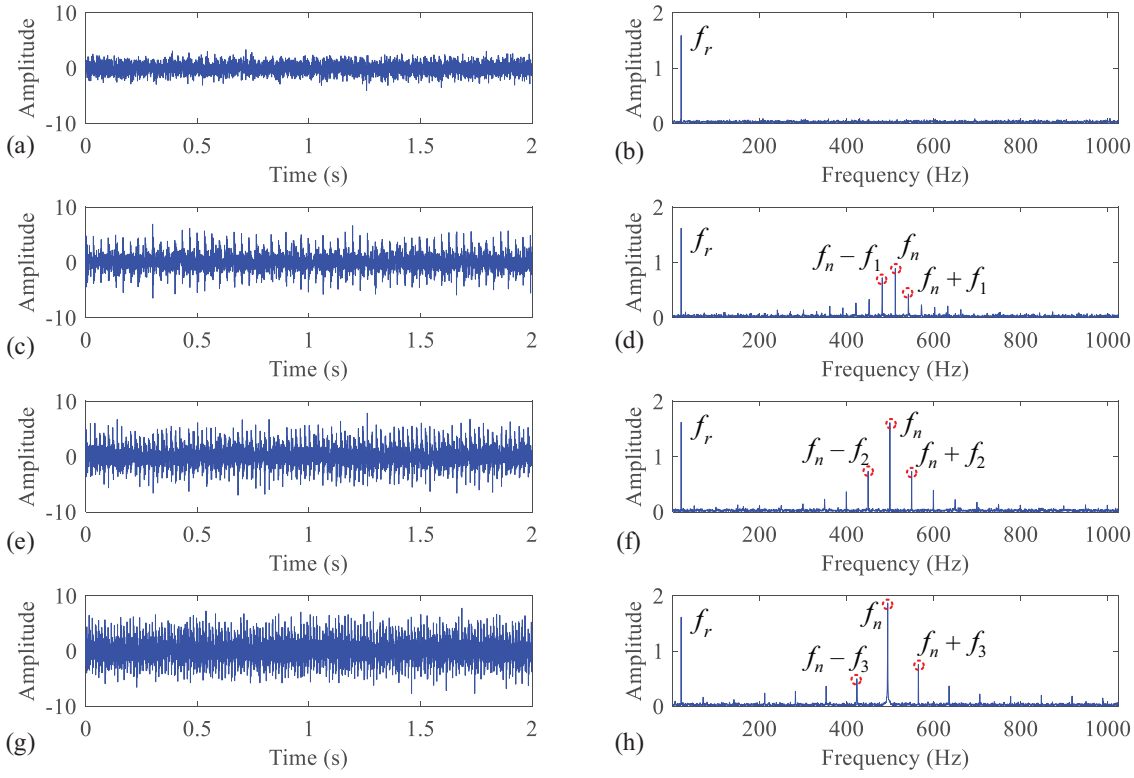

Fig. 3. (a) and (b) The simulated signal in a healthy condition and its FS; (c) and (d) the simulated signal with fault characteristic frequencies at 30 Hz and its FS; (e) and (f) the simulated signal with fault characteristic frequencies at 50 Hz and its FS; (g) and (h) the simulated signal with fault characteristic frequencies at 70 Hz and its FS.

where $\Sigma_{i=1}^{\lfloor N/T_a \rfloor} A_k \delta(t - iT_k) * s_k(t)$ represents cyclic impulse responses excited by defects; T_k denotes the time interval of the cyclic impulse, and $f_k = 1/T_k$ is the fault characteristic frequency (FCF), where different FCFs are assigned to simulate pitting faults in various parts of the bearing; $s_i = e^{-\eta t}\sin(2\pi f_n t)$ is the impulse response of the SDOF, and $\eta = f_n\xi/\sqrt{1-\xi^2}$; f_n and ξ represent the natural frequency and the damping ratio of the SDOF; $B_r\cos(2\pi k f_r t)$ is periodic interferences, which can be regarded as interferential components, with frequency f_r, which exists in both healthy and faulty conditions; and white noise $n(t)$ stands for external interferences.

In this numerical experiment, the sample frequency and signal length are 2048 Hz and 4096; f_n and ξ are set to 500 Hz and 0.05; and the frequency of periodic interferences is 20 Hz and its amplitude coefficient B_r is 1.6. In addition, three fault components at characteristic frequencies of $f_1 = 30\,\text{Hz}$, $f_2 = 50\,\text{Hz}$, and $f_3 = 70\,\text{Hz}$ are included, the amplitude coefficient A_k for each component is set to 5. The simulated signals are shown in Fig. 3.

Subsequently, the multiclass OWS is calculated according to the optimization model, where the regular coefficient is set to 0.1. Figure 4 presents the weight distributions of the multiclass OWS under different FCFs. As shown in Fig. 4(a), in the healthy case, the OWS allocates significant positive weights at the frequency of 20 Hz, which corresponds to periodic interference present in all signals. When fault components are introduced, as shown in Fig. 4(b–d), the OWS consistently assigns positive weights at the frequencies around 500 Hz with an interval of FCFs (marked in red). These positive weights signify the discriminative performance of OWS in enhancing fault-relevant spectral components. Notably, the interference frequency at 20 Hz remains a negative weight in all cases except the healthy one, which further verifies that the OWS successfully separates meaningful fault information from misleading components.

Moreover, as the fault frequency increases from 30 Hz to 70 Hz, intervals of corresponding dominant positive weights shift accordingly. This behavior also validates the interpretability of the multiclass OWS: positive weights are assigned to characteristic frequencies associated with the corresponding class, while negative weights are allocated to characteristic frequencies of other classes (frequencies of interferential components can be regarded as the characteristic frequencies of the healthy condition).

These results verify that the multiclass OWS framework is capable of distinguishing between fault-related components and interference components by allocating them distinct weight signs. This capability is crucial for achieving interpretable fault detection in multi-fault scenarios.

IV. EXPERIMENTAL VALIDATIONS USING THE XJTU BEARING DATASET

To evaluate the multiclass classification model-based OWS under realistic diagnostic settings, the XJTU-SY run-to-failure dataset is employed. This dataset originates from accelerated degradation experiments on rolling bearings

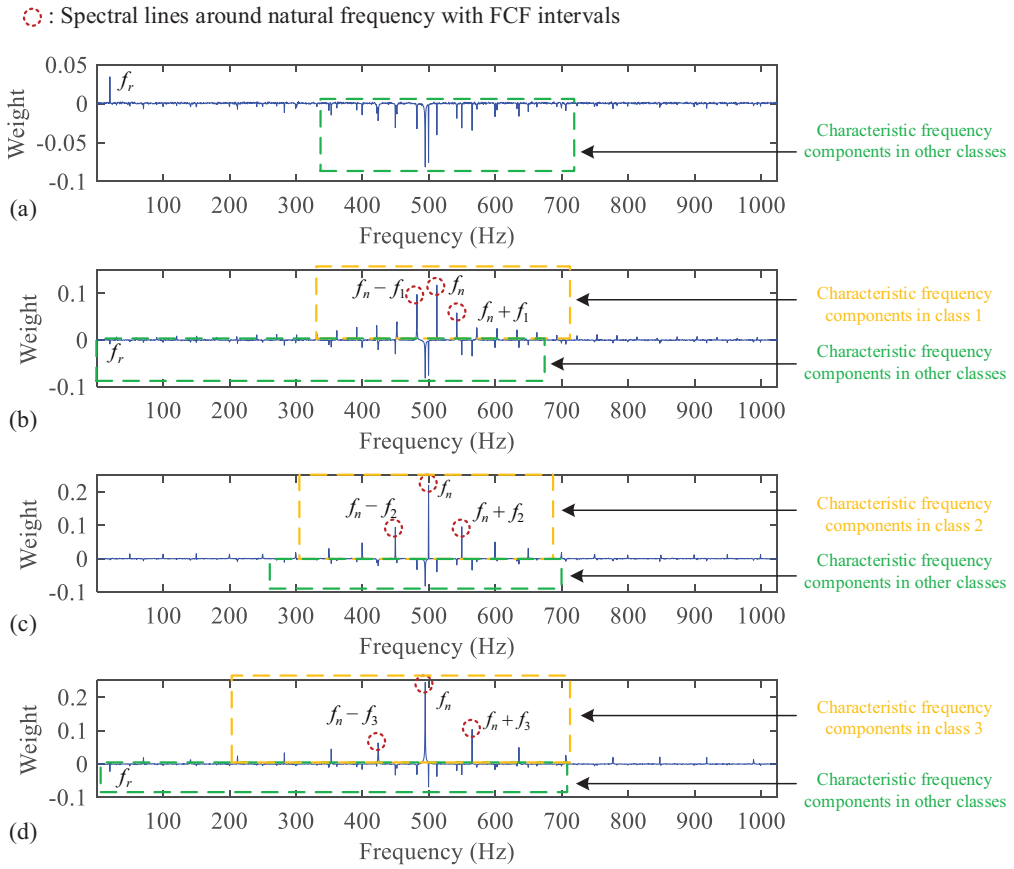

Fig. 4. Multiclass OWS for each class: (a) healthy condition; (b) faulty condition with FCF of 30 Hz; (c) faulty condition with FCF of 50 Hz; (d) faulty condition with FCF of 70 Hz.

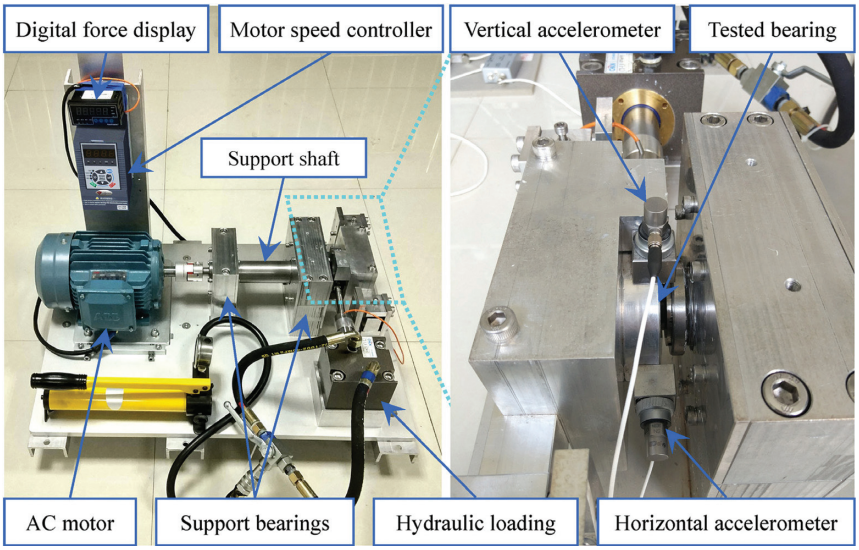

Fig. 5. Experimental rig of XJTU-SY dataset.

Table I. Fault characteristic frequencies and rotational frequency under Condition 2

Rotational frequency	BPFO	BPFI	FTF
$f_r = 37.5$ Hz	$f_o = 115.6$ Hz	$f_i = 184.4$ Hz	$f_t = 14.5$ Hz

carried out in a controlled laboratory environment. In this study, the experimental platform is configured to simulate real-world bearing wear progression and includes hydraulic loading and dual-axis vibration acquisition, as illustrated in Fig. 5.

Among the three operating conditions available in the dataset, Condition 2 is selected for this validation, involving a radial load of 11 kN and a shaft speed of 2250 rpm. Under this condition, three test bearings, identified as 2_1, 2_2, and 2_3, are chosen for the multiclass classification model-based OWS analysis. The failure patterns varied across the three bearings, involving inner-race damage, outer-race degradation, and cage fault, respectively. Theoretical FCFs were calculated for these defects, namely the ball-pass frequency of the inner race (BPFI), the ball-pass frequency of the outer race (BPFO), and the fundamental train frequency (FTF). In addition, the rotational frequency is also provided. All these theoretical FCFs are summarized in Table I.

These diverse failure modes offer a representative validation set for multi-type fault diagnosis. As the loading direction is horizontal, only the horizontal axis signals are used in this study, which have been shown to carry more fault-related information. Data were acquired at a sampling rate of 25.6 kHz. Each record consists of 32,768 samples, corresponding to a time length of 1.28 s per acquisition.

Before implementing the multiclass OWS, samples are labeled according to their corresponding health conditions. Specifically, the first ten samples of each of the three bearings are labeled as a healthy condition. Fault samples are selected as follows: samples 461–470 from Bearing 2_1 represent an inner race fault, samples 151–160 from Bearing 2_2 correspond to an outer race fault, and samples 501–510 from Bearing 2_3 correspond to a cage fault.

Since the squared envelope is employed to address potential signal modulation, the SES is subsequently used to compute the multiclass OWS. The SES of the selected samples is presented in Fig. 6, where the FCFs and their harmonics are marked. It is noteworthy that among various fault types, in addition to the evident FCFs, there also exist many other prominent spectral lines in the SES, as illustrated in Fig. 6(d), which may be attributed to the complex mechanical structures and failure processes. Although these prominent spectral lines in SES may not align with the theoretical FCFs, they can still serve as valuable evidence for fault diagnosis.

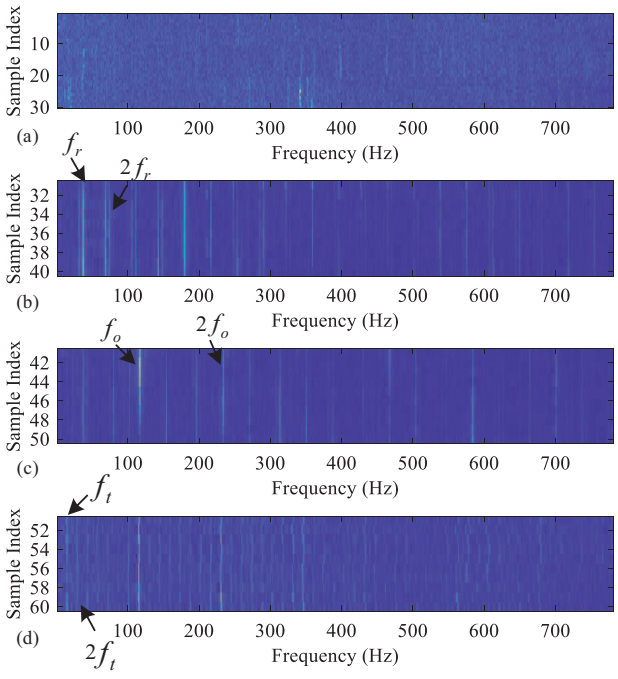

Fig. 6. SES of different conditions: (a) healthy condition; (b) inner race fault; (c) outer race fault; (d) cage fault.

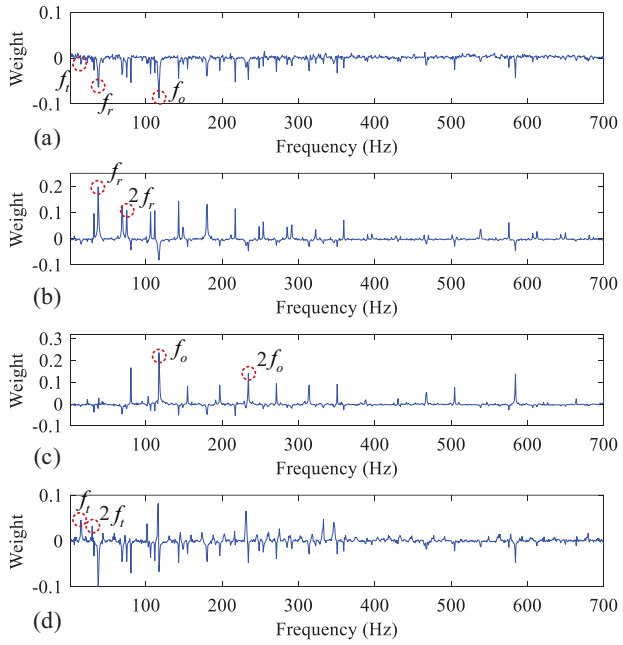

Fig. 7. Multiclass OWS for each health condition: (a) healthy condition; (b) inner race fault; (c) outer race fault; and (d) cage fault.

As illustrated in the figure, the SES of the healthy samples does not exhibit any prominent spectral components. In contrast, all three fault types show prominent spectral lines in their SES, each associated with their respective characteristic frequencies, along with multiple harmonics. For the inner race fault and cage fault, theoretical FCFs are clearly visible and dominant in the SES, demonstrating strong spectral responses at the expected fault frequencies. However, in the case of the outer race fault, the expected FCF is not clearly manifested. Instead, the rotational frequency and its harmonics appear prominently. Despite the absence of the theoretical FCF, this frequency pattern can still serve as a useful indicator for identifying the fault type.

After calculating the multiclass OWS based on the optimization model, the obtained weight distributions align well with the theoretical analysis, as shown in Fig. 7. Regarding the multiclass OWS of the healthy condition, no prominent positive weights are observed, which is consistent with their SES, where no significant spectral components are present. Instead, the negative weights in the OWS correspond to the FCFs and their harmonics associated with other faulty types. For each specific fault type, the multiclass OWS assigns positive weights to its own FCFs (not only the theoretical FCFs but also other fault-related frequency components introduced by practical faults), while negative weights correspond to the FCFs of other fault types. These positive spectral lines are consistent with previous observations and confirm that the method captures fault-specific spectral patterns while suppressing irrelevant or misleading components from other health conditions.

V. CONCLUSIONS

In recent years, interpretable modeling approaches have drawn increasing attention in the field of machinery condition monitoring, and the earlier binary OWS framework was able to differentiate fault-related and fundamental frequencies through the assignment of positive and negative spectral weights, showing great potential for practical machinery condition monitoring. Considering that multiclass classification is often met in practical scenarios, this work extended the original OWS to multiclass classification model-based OWS. The softmax classifier is first applied to solve the model and obtain multiclass OWS, and the property of the proposed multiclass OWS is studied and further validated with a numerical case. Finally, the effectiveness of the multiclass classification model-based OWS was demonstrated through experiments on a bearing dataset. The multiclass OWS, as interpretable machine learning fault features that are directly connected with informative frequency bands or FCFs, provide new insight for spectrum-based fault classification models and are capable of revealing both distinctive fault-related frequencies and fundamental frequency components. The difference between the original binary OWS and the studied multiclass OWS is that negative spectral lines may represent not only from interferential components but also fault components of other classes.

ACKNOWLEDGMENTS

This work was supported by the National Natural Science Foundation of China under Grant Nos. 523B2043 and 52475112.

CONFLICT OF INTEREST STATEMENT

The authors declare no conflicts of interest.

REFERENCES

[1] Y. Lei, N. Li, L. Guo, N. Li, T. Yan, and J. Lin, "Machinery health prognostics: A systematic review from data acquisition to RUL prediction," *Mechanical Systems and Signal Processing*, vol. 104, pp. 799–834, 2018, doi: 10.1016/j.ymssp.2017.11.016.

[2] Z. Chen, H. Wang, Y. Zhou, Y. Yang, and Y. Liu, "A multiscale feature extraction and fusion method for diagnosing bearing faults," *Journal of Dynamics, Monitoring and Diagnostics*, Aug. 2024, doi: 10.37965/jdmd.2024.560.

[3] R. B. Randall,*Vibration–Based Condition Monitoring*. Wiley, 2021. doi: 10.1002/9781119477631.

[4] M. Feldman, "Hilbert transform in vibration analysis," *Mechanical Systems and Signal Processing*, vol. 25, no. 3, pp. 735–802, 2011, doi: 10.1016/j.ymssp.2010.07.018.

[5] R. B. Randall and J. Antoni, "Choosing the right signal processing tools for mechanical systems," *Mechanical Systems and Signal Processing*, vol. 224, p. 112090, 2025, doi: 10.1016/j.ymssp.2024.112090.

[6] Y. Wang, G. Xu, A. Luo, L. Liang, and K. Jiang, "An online tacholess order tracking technique based on generalized demodulation for rolling bearing fault detection," *Journal of Sound and Vibration*, vol. 367, pp. 233–249, 2016, doi: 10.1016/j.jsv.2015.12.041.

[7] W. A. Gardner, "Measurement of spectral correlation," *IEEE Transactions on Acoustics, Speech, and Signal Processing*, vol. 34, no. 5, pp. 1111–1123, 1986, doi: 10.1109/TASSP.1986.1164951.

[8] J. Antoni, G. Xin, and N. Hamzaoui, "Fast computation of the spectral correlation," *Mechanical Systems and Signal Processing*, vol. 92, pp. 248–277, 2017, doi: 10.1016/j.ymssp.2017.01.011.

[9] J. Antoni, "Fast computation of the kurtogram for the detection of transient faults," *Mechanical Systems and Signal Processing*, vol. 21, no. 1, pp. 108–124, 2007, doi: 10.1016/j.ymssp.2005.12.002.

[10] N. Sawalhi, R. B. Randall, and H. Endo, "The enhancement of fault detection and diagnosis in rolling element bearings using minimum entropy deconvolution combined with spectral kurtosis," *Mechanical Systems and Signal Processing*, vol. 21, no. 6, pp. 2616–2633, 2007, doi: 10.1016/j.ymssp.2006.12.002.

[11] Y. Wang, J. Xiang, R. Markert, and M. Liang, "Spectral kurtosis for fault detection, diagnosis and prognostics of rotating machines: A review with applications," *Mechanical Systems and Signal Processing*, vol. 66–67, pp. 679–698, 2016, doi: 10.1016/j.ymssp.2015.04.039.

[12] Y. Miao *et al.*, "A review on the application of blind deconvolution in machinery fault diagnosis," *Mechanical Systems and Signal Processing*, vol. 163, p. 108202, 2022, doi: 10.1016/j.ymssp.2021.108202.

[13] R. B. Randall and J. Antoni, "Why EMD and similar decompositions are of little benefit for bearing diagnostics," *Mechanical Systems and Signal Processing*, vol. 192, p. 110207, 2023, doi: 10.1016/j.ymssp.2023.110207.

[14] J. Antoni, "A critical overview of the 'filterbank-feature-decision' methodology in machine condition monitoring," *Acoustics Australia*, vol. 49, no. 2, pp. 177–184, 2021, doi: 10.1007/s40857-021-00232-7.

[15] Y. Miao, B. Zhang, C. Li, J. Lin, and D. Zhang, "Feature mode decomposition: New decomposition theory for rotating machinery fault diagnosis," *IEEE Transactions on Industrial Electronics*, vol. 70, no. 2, pp. 1949–1960, 2023, doi: 10.1109/TIE.2022.3156156.

[16] B. Hou, M. Xie, H. Yan, and D. Wang, "Impulsive mode decomposition," *Mechanical Systems and Signal Processing*, vol. 211, p. 111227, 2024, doi: 10.1016/j.ymssp.2024.111227.

[17] B. Hou, Y. Wang, and D. Wang, "Cycle-embedded sparsity measures as a generalized objective function of impulsive mode decomposition for impulsive fault component extraction," *Mechanical Systems and Signal Processing*, vol. 231, p. 112566, 2025, doi: 10.1016/j.ymssp.2025.112566.

[18] Y. Lei, B. Yang, X. Jiang, F. Jia, N. Li, and A. K. Nandi, "Applications of machine learning to machine fault diagnosis: A review and roadmap," *Mechanical Systems and Signal Processing*, vol. 138, p. 106587, 2020, doi: 10.1016/j.ymssp.2019.106587.

[19] Y. LeCun, Y. Bengio, and G. Hinton, "Deep learning," *Nature*, vol. 521, no. 7553, pp. 436–444, 2015, doi: 10.1038/nature14539.

[20] L. Guo, N. Li, F. Jia, Y. Lei, and J. Lin, "A recurrent neural network based health indicator for remaining useful life prediction of bearings," *Neurocomputing*, vol. 240, pp. 98–109, 2017, doi: 10.1016/j.neucom.2017.02.045.

[21] S. Shao, S. McAleer, R. Yan, and P. Baldi, "Highly accurate machine fault diagnosis using deep transfer learning," *IEEE Transactions on Industrial Informatics*, vol. 15, no. 4, pp. 2446–2455, 2019, doi: 10.1109/TII.2018.2864759.

[22] T. Li *et al.*, "WaveletKernelNet: An interpretable deep neural network for industrial intelligent diagnosis," *IEEE Transactions on Systems, Man, and Cybernetics: Systems*, vol. 52, no. 4, pp. 2302–2312, 2022, doi: 10.1109/TSMC.2020.3048950.

[23] B. An, S. Wang, F. Qin, Z. Zhao, R. Yan, and X. Chen, "Adversarial algorithm unrolling network for interpretable mechanical anomaly detection," *IEEE Transactions on Neural Networks and Learning Systems*, vol. 35, no. 5, pp. 6007–6020, 2024, doi: 10.1109/TNNLS.2023.3250664.

[24] Q. Chen *et al.*, "TFN: An interpretable neural network with time-frequency transform embedded for intelligent fault diagnosis," *Mechanical Systems and Signal Processing*, vol. 207, p. 110952, 2024, doi: 10.1016/j.ymssp.2023.110952.

[25] D. Wang, Z. Peng, and L. Xi, "The sum of weighted normalized square envelope: A unified framework for kurtosis, negative entropy, Gini index and smoothness index for machine health monitoring," *Mechanical Systems and Signal Processing*, vol. 140, p. 106725, 2020, doi: 10.1016/j.ymssp.2020.106725.

[26] B. Hou, D. Wang, Y. Chen, H. Wang, Z. Peng, and K.-L. Tsui, "Interpretable online updated weights: Optimized square envelope spectrum for machine condition monitoring and fault diagnosis," *Mechanical Systems and Signal Processing*, vol. 169, p. 108779, 2022, doi: 10.1016/j.ymssp.2021.108779.

[27] B. Hou, D. Wang, J.-Z. Kong, J. Liu, Z. Peng, and K.-L. Tsui, "Understanding importance of positive and negative signs of optimized weights used in the sum of weighted normalized Fourier spectrum/envelope spectrum for machine condition monitoring," *Mechanical Systems and Signal Processing*, vol. 174, p. 109094, 2022, doi: 10.1016/j.ymssp.2022.109094.

[28] B. Hou, D. Wang, Z. Peng, and K.-L. Tsui, "Adaptive fault components extraction by using an optimized weights spectrum based index for machinery fault diagnosis," *IEEE Transactions on Industrial Electronics*, vol. 71, no. 1, pp. 985–995, 2024, doi: 10.1109/TIE.2023.3243282.

[29] B. Sun, H. Li, J. Wang, S. Chen, Y. Yang, and Z. Ma, "Adaptive fault components extraction based on physically interpretable optimized weight time–frequency matrix index and its applications in rotating machinery fault diagnosis," *Structural Health Monitoring*, p. 14759217241303161, 2025, doi: 10.1177/14759217241303161.

[30] B. Hou, D. Wang, T. Xia, Z. Peng, and K.-L. Tsui, "Difference mode decomposition for adaptive signal decomposition," *Mechanical Systems and Signal Processing*, vol. 191, p. 110203, 2023, doi: 10.1016/j.ymssp.2023.110203.

[31] J. Guo, Y. Liu, R. Yang, W. Sun, and J. Xiang, "Differgram: A convex optimization-based method for extracting optimal frequency band for fault diagnosis of rotating machinery," *Expert Systems with Applications*, vol. 245, p. 123051, 2024, doi: 10.1016/j.eswa.2023.123051.

[32] T. Meng, X. Jiang, S. Yang, J. Liu, H. Gao, and Z. Zhu, "Spectral feature-informed difference multi-modes decomposition for compound bearing fault diagnosis," *Expert Systems with Applications*, vol. 294, p. 128735, 2025, doi: 10.1016/j.eswa.2025.128735.

[33] Y. Wang, D. Wang, B. Hou, S. Lu, and Z. Peng, "Robust optimized weights spectrum: Enhanced interpretable fault feature extraction method by solving frequency fluctuation problem," *Mechanical Systems and Signal Processing*, vol. 222, p. 111798, 2025, doi: https://doi.org/10.1016/j.ymssp.2024.111798.

[34] T. Hastie, R. Tibshirani, and J. H. Friedman,*The Elements of Statistical Learning: Data Mining, Inference, and Prediction*, Second edition. Springer Series in Statistics. New York, NY: Springer, 2017.

[35] F. Hou, J. Chen, and G. Dong, "Weak fault feature extraction of rolling bearings based on globally optimized sparse coding and approximate SVD," *Mechanical Systems and Signal Processing*, vol. 111, pp. 234–250, 2018, doi: 10.1016/j.ymssp.2018.04.003.